Room temperature sintering of polar ZnO nanosheets: I-Evidence

Amparo Fernández-Pérez, Verónica Rodríguez-Casado, Teresa Valdés-Solís and Gregorio Marbán♣

Instituto Nacional del Carbón (INCAR-CSIC) – c/Francisco Pintado Fe 26, 33011-Oviedo (Spain).

Tel. +34 985119090; Fax +34 985297662

Abstract

Polar ZnO nanosheets of high specific surface area (~120 m^2/g) were subjected to storage under different atmospheres at room temperature and analyzed for changes in their textural and crystal properties. During their storage in laboratory conditions (in closed transparent polypropylene vials kept under the light of the laboratory on worktop tables) the nanosheets lost up to 75% of their specific surface area in approximately two months, with most of the loss occurring during the first two weeks. The narrow mesoporosity (~5 nm pore size) became filled with ZnO during the process. No loss or gain in weight was detected. Loss of specific surface area took place under all of the atmospheres assayed, in the following order: moist air (with or without light) > moist CO_2-free atmosphere (with or without light and/or oxygen) > dry CO_2-free oxygen-containing atmosphere (with or without light) > dry inert atmosphere (with light) > dry inert atmosphere (in darkness). During storage the ZnO crystals grew mainly by the partial merging of their polar surfaces in a process triggered by the action of moisture, oxygen and, in the absence of these two agents, light. The mechanism of this intriguing phenomenon will be analyzed in detail in the second part of this work.

Keywords: ZnO, polar nanosheets, specific surface area, crystal size, XRD

♣ Corresponding author: greca@incar.csic.es

Introduction

ZnO nanostructures have been the subject of a large number of studies and reviews [1, 2] due to their important role in the fields of electronics, optics and photonics. It is well known that the surfaces of ZnO nanostructures can be chemically altered at room temperature by the prevailing atmosphere and that this leads to the formation of surface hydroxyls [3, 4] or to the loss of oxygen vacancies [5]. On the other hand, to our knowledge, no systematic study has been devoted to date to the analysis of the possible effect of atmospheric storage on the specific surface area of the ZnO materials, even though there is indirect evidence in the literature of unexpected changes of this parameter in commercially available ZnO powders [6]. Unfortunately, in the descriptions of the analyses to which these materials were subjected, most authors (ourselves included) have not usually reported how they were stored or preserved during the experimental procedure, or whether the storing conditions might have altered the specific surface area of the ZnO nanostructures. This was the reason, in fact, that prompted us to undertake the present study. We observed that several stainless steel wire mesh-supported ZnO samples described in some of our works [7-10], prepared according to a well-controlled procedure, showed random values of specific surface area in the 35-110 m^2/g range, with an average value of ~80 m^2/g, as reported in the works mentioned above. As the only uncertain variable in these works was the storage time between calcination and surface area analysis, we performed a systematic analysis of the effect of storage under different conditions upon the specific surface area and crystal properties of ZnO.

Room temperature sintering of ZnO may have relevance in the fields in which the specific surface area is an important property of the material (catalysis, adsorption, etc.); the fact that the specific surface area of the particles may suffer an unexpected variation during storage inevitably leads to a misinterpretation of the experimental results when this alteration is not considered. Besides, the control of this process may have potential applications, such as the fabrication of ZnO ink formulations for sinter-free printing of semiconductive films, in a similar way as silver nanoparticles

are currently being used for printing conductive circuits [11-13]. The purpose would be to produce an ink of polar ZnO nanoparticles, stabilized by an appropriate organic agent, whose removal upon deposition of the printed pattern would trigger the spontaneous sintering of the ZnO nanoparticles under the appropriate moist atmosphere at room temperature to form the semiconductive film.

This work is divided into two parts, the first of which provides evidence of the room temperature sintering of polar ZnO, and of the effect of the prevailing atmosphere upon the apparently inexplicable loss of specific surface area. The second part of this work attempts to explain the proposed mechanism behind this phenomenon.

Experimental

Sample preparation

All of the chemical reagents were of analytical grade and hence did not require additional purification. All of the aqueous solutions were prepared with deionized water. The support was a stainless steel wire mesh [SSWM , with a 36 μm wire diameter and 42 μm mesh screen openings] supplied by CISA Cedacería Industrial (www.cisa.net). The SSWM-supported ZnO samples with a yield of ZnO of ~20 wt.% were synthesized following roughly the same procedure as that described in [9]. Briefly, zinc acetate dihydrate was dissolved together with urea in deionized water. A Zn^{2+} concentration of 0.05 M was used in the aqueous solution, at an urea/Zn^{2+} molar ratio of 20. The pH of the solution was adjusted to 4.88 by using acetic acid (1.2 M). The wire mesh was placed in a Teflon autoclave (100 ml) filled to the top with the growth solution. The autoclave was sealed and the growth of hydrothermal ZnO was allowed to proceed at 80°C for 23 h in a furnace. The ZnO coated-wire mesh was then taken out of the solution, thoroughly washed with deionized water, immersed in an ultrasonic bath for 10 min and vacuum-dried at 60°C. Finally the sample was calcined at 210°C for 1.0 h in air, cooled in the furnace at a rate of ~1°C/min and stored under

controlled conditions for further analysis. The time zero for storage was taken to be that of the conclusion of the cooling ramp. The SSWM-supported ZnO sample was denominated ZnO-M (from mesh; Figure 1A). For some analyses, groups of ZnO nanosheets were gently scratched from the wire mesh surface with a brush and then disaggregated in a mortar. The resulting powder was denominated ZnO-P (Figure 1B).

Sample storage

Different storage conditions for the calcined samples were studied, as described below.

Storage in lab conditions: the standard storage of the samples and the source of random values of specific surface area in past works, in closed transparent polypropylene vials kept under the light of the laboratory on worktop tables.

Unprotected storage: samples on open Petri dishes kept under the light of the laboratory on worktop tables.

Storage under gas flows: samples kept in Vis/UV transparent devices, either under the light of the laboratory or in darkness, subjected to a 100 mL/min flow of gas [dry helium, moist helium (bubbled through a water bath), dry air, moist air, dry 21%O_2/He and moist 21%O_2/He stream].

Characterization techniques

The morphology of the samples was studied by means of scanning electron microscopy (SEM, FEI Quanta FEG 650 model). Transmission electron micrographs (TEM) were taken on a JEOL (JEM-2000 EX II) microscope operating at 160 kV. Selected Area Electron Diffraction (SAED) patterns were obtained from representative areas of the TEM images. The X-ray diffraction (XRD) patterns of the samples were recorded on a Bruker D8 Advance instrument operating at 40 kV and 40 mA using

Cu Kα radiation (λ = 0.15406 nm). The crystal size values were estimated from the XRD pattern by means of Scherrer's equation (d_{100} or d_{002} are crystal diameters evaluated from peaks (100) and (002), respectively, of the ZnO pattern). The BET specific surface area of the samples was evaluated from N_2 adsorption isotherms (-196ºC) obtained with a Micromeritics ASAP 2020 analyser. The BET surface area was deduced from an analysis of the isotherms in the relative pressure range of 0.04 to 0.20. Pore size distribution (PSD) was calculated by applying the Kruk-Jaroniec-Sayari method [14] to the desorption branch. In specific cases (Figure 4B) the BET surface area was evaluated from single point measurements on a Micomeritics Autochem II chemisorption analyser.

Results and Discussion

Freshly calcined samples

Figure 2 shows XRD spectra of the freshly calcined ZnO-M and ZnO-P samples (SEM images of these samples are shown in Figs. 1A and 1B, respectively). The wide peaks observed in the XRD spectra correspond to very small crystal sizes of around 10 nm. The XRD pattern for hexagonal wurtzite-type ZnO (JCPDS No. 36-1451) has three main peaks at 2θ = 31.8, 34.4 and 36.3° (see bars in Fig. 2A), representative of, respectively [15]: (a) a non-polar crystal plane $(10\bar{1}0)$ [or (100)], with a separation distance between parallel planes of ~0.28 nm (these planes form the long surfaces, parallel to the c axis, of typical ZnO nanorods, illustrations of which are displayed in Figure 3); (b) a polar crystal plane (0002) [or (002)] which is considered to be equivalent to the Zn-terminated positive polar plane (0001) or the O-terminated negative polar plane $(000\bar{1})$, with a separation distance between the parallel planes of ~0.26 nm (typical basal planes, normal to the c axis, that form the top and bottom surfaces, respectively, of ZnO nanorods), and (c) a polar crystal plane $(10\bar{1}1)$ [or (101)], with a separation distance between the parallel planes of ~0.24 nm, which is the plane that forms the surfaces of hexagonal pyramids sometimes found at the top of ZnO nanorods [15].

The polarity of ZnO wurtzite-type nanostructures is thought to be related to the intensity ratio of (002) to (100) peaks (I_{002}/I_{100}) in the XRD spectra [16]. However, on this point the literature offers conflicting conclusions. For instance, the criterion used by Li et al. [17] (that I_{002}/I_{100} increases with polarity) is opposite to that of McLaren et al. [16] (that I_{002}/I_{100} decreases with polarity). In the present work, a way to conciliate both criteria is examined. Given their geometry (nanorods, nanoflakes, needles, pyramids, etc.) and their degree of anisotropy, single crystalline ZnO nanostructures may have different ratios of polar to non-polar surfaces, that is, different overall polarities. According to Han et al. [15], the least polar material (nanocolumns or nanorods in their work) has the lowest I_{002}/I_{100} ratio, a result which, in principle, agrees with the assessment of Li et al. [17]. However, assuming that ZnO rods (or nanorods) with a high aspect ratio, oriented along the c axis, are eminently composed of non-polar surfaces with (hl0) Miller indexes, examples in the literature can be found of different XRD peak ratios (I_{002}/I_{100}) for similar nanorod-type samples (both $I_{002}/I_{100}<1$ [15, 17, 18] and $I_{002}/I_{100}>1$ [16, 19-21]). According to Tian et al. [21] the more marked growth in intensity of the (002) peak, compared to that of the (100) peak, is due to the alignment of the nanorods, which results in the (002) plane being preferentially exposed. It is for this reason that XRD patterns of seeded nanorods at different stages of growth show a low I_{002}/I_{100} value at the beginning of the process, when the nanorods are randomly oriented, but a I_{002}/I_{100} value greater than 1 when the growth process has been completed and the nanorods have become parallel. Among the $I_{002}/I_{100}>1$ materials the same alignment is observed in [19] (in this case via self-assemblage, as the nanorods were not grown on a substrate) and also, though not so well developed, in [20]. On the other hand, among the samples with I_{002}/I_{100} values below 1, there is a random orientation in the above examples, [15, 17, 18], as can be appreciated from the SEM images where the nanorods look like fields of randomly oriented felled trees.

It is clear that the I_{002}/I_{100} ratio depends on alignment and orientation just as much as it depends on the polarity (and degree of anisotropy) of the material. Thus, the non-polar (100) plane is mainly

exposed in XRD when the non-polar nanorods are randomly oriented (unsupported nanorods), that is, when the surfaces represented by this and other (hk0) planes are mostly parallel to the base of the sample holder (which resembles a field of randomly oriented felled trees, as already mentioned) and therefore the I_{002}/I_{100} ratio obtained is always below 1 [3, 15, 17, 18, 22]. Only in one case among those analyzed from the literature was a I_{002}/I_{100} ratio over 1 found for ZnO nanorods with a "felled tree" alignment (ZnO needles in [4]). However, the peak area ratio in this particular case, A_{002}/A_{100}, is clearly below one, and therefore the cumulative counts per second are larger in the case of the (100) plane than for the (002) plane, as one would expect for "felled tree" orientation. On the other hand, supported or self-assembled nanorods that are aligned so that their polar tips are parallel to the base of the sample holder always show I_{002}/I_{100} ratios greater than 1 [19-21, 23-26]. This relationship between the orientation of the nanorods and the I_{002}/I_{100} ratio is highlighted even more in the work of Vu et al. [27]. Other non-polar nanostructures different to nanorods also offer the same result; i.e. aligned non-polar nanosheets with the (002) edge parallel to the base of the XRD sample holder result, as expected, in an I_{002}/I_{100} ratio over 1 [28]. A pictorial representation of this conclusion is presented in Figure 3, which shows how the same nanostructures (i.e. nanorods) can produce XRD patterns with different I_{002}/I_{100} ratios simply by changing their orientation.

To return to the ZnO-M and ZnO-P samples, they offer rather different I_{002}/I_{100} ratios immediately after calcination; between 0.29 (inset of Figure 2A) and 0.56 for ZnO-M (average 0.42±0.10) and between 0.81 (inset of Figure 2B) and 1.10 for ZnO-P (average 0.93±0.12). These values together with the above conclusions suggest that ZnO-M consists mainly of polar nanosheets with a polycrystalline appearance that are aligned normal to the wire mesh surface (Figure 1A), with the (100) non-polar facets of the crystals that form their edges being left exposed (like the aligned nanoflakes when $I_{002}/I_{100}<1$ in Figure 3). The material scratched from the wire mesh (ZnO-P), consists of both nanosheets and the more amorphous material that connects the nanosheets with the wire mesh. All of this particulate material becomes randomly oriented when deposited on the holder

(Figure 1B), and the polar nanosheets preferentially leave the (002) polar surfaces of their crystals exposed, which results in a significant increase in the I_{002}/I_{100} ratio (in the same way the "deposited" nanoflakes result in $I_{002}/I_{100}>1$ in Figure 3). The crystal sizes evaluated for the (100) and (002) peaks differ by about 0.5 nm [$d_{002} = d_{100} + (0.5 \pm 0.1)$], regardless of the storage time and sample type (ZnO-M or ZnO-P). This indicates that, on average, the polar (002) contribution to the surface area of the crystals is slightly higher than the non-polar (100) contribution. Figure 4A shows a TEM image of the main surface of a freshly calcined ZnO nanosheet. The sheet is formed by an assembly of irregular crystals with a size of around 10 nm. A SAED analysis of this surface shows typical diffraction points for (100) facets (separated by a distance of 0.28 nm), (002) facets (separated by a distance of 0.26 nm) and (101) facets (separated by a distance of 0.24 nm). According to the different intensities of the diffraction points, the most exposed facet is (002) (the ratio $I_{0.28\ nm}/I_{0.26\ nm}$ indicated in Figure 4B being directly related to the I_{002}/I_{100} ratio in XRD), thus confirming the polar character of the main surface of the ZnO nanosheets. Figure 4C shows that the crystals that form the nanosheet leave space for regularly distributed mesopores of about ~5 nm in size. It should also be pointed out that, in spite of the low calcination temperature used to prepare the material (210°C), the degrees of crystallinity (DOC) evaluated from the XRD patterns [29] are 63% and 78% for ZnO-M and ZnO-P, respectively.

Loss of specific surface area during storage at different conditions

Figure 5 shows N_2 physisorption isotherms on a ZnO mass basis for the freshly calcined ZnO-M and for the same sample after being stored in lab conditions for 40 days. Unexpected differences in both isotherms, to our knowledge never reported before for nanostructured ZnO materials, are clearly visible. After 40 days' storage the amount of physisorbed N_2 has decreased notably and the pore size distribution (inset in Figure 5) has changed from a bimodal distribution (5.9 and 68 nm) to a unimodal one (69 nm), with a certain degree of densification (the pore volume has diminished from

0.3 to 0.2 cm^3/g), evidencing that the narrow mesopores (~6 nm), already detected in the TEM analysis (Fig. 4C), have coalesced during storage. No loss or gain of ZnO mass during the process was detected. Pending the spectroscopic characterization, that will be reported in the second part of this work, it can be conjectured that this result is due to the diffusion of zinc from the surfaces adjacent to the macropores (>50 nm) towards the surfaces delimiting the mesopores, probably via grain boundary defects. Figure 6 shows the evolution of the loss of specific surface area of ZnO-M (on a ZnO mass basis) during storage in different conditions. The freshly calcined sample has a specific surface area in the range 115-130 m^2/g. After more than two months of storage in lab conditions the specific surface area of the sample has decreased to a value of ~33 m^2/g (~72% surface area loss). As can be seen from the figure, most of the surface reduction took place within the first two weeks, accompanied by an increase in crystal size, the magnitude of which depends on the orientation of the nanoparticles. This can be appreciated in Figures 2A and 2B, from the samples kept under unprotected storage. At the edges of the nanosheets, the crystal size evaluated by applying Scherrer's equation (inset in Figure 2A) ranges from 10.0[10.5] nm (d_{100}[d_{002}]) at 0 days' storage to 13.7[13.9] nm after 15 days' storage, whereas the crystal size evaluated for the ZnO-P sample, which leaves the most extensive nanosheet surface exposed, ranges from 9.7[10.2] nm at 0 days to 12.4[13.0] nm after 15 days' storage (inset in Figure 2B). Such preferential growth might occur either because the nanosheets are very thin, especially at the edges, crystal growth being favoured in these thin areas, or because the edges of the nanosheets in the ZnO-M sample (Figure 1A) are more directly exposed to light during storage than the surfaces of the ZnO-P sample, which are partially shaded by the accumulation of nanosheets (Figure 1B). However, this effect must be discarded given the experimental evidence presented in Figure 7, which shows the results of specific surface area loss for ZnO-M samples after 4 days' storage under different gas and lighting conditions. From the data shown in the figure it can be concluded that:

- Only under a dry He atmosphere does light have a significant effect, with a loss in specific surface area after four days of 14.6 ± 5.2%, under the light of the laboratory, and of 4.8 ± 3.5% in darkness; values which, in any case, are much lower than those obtained in the presence of oxygen and/or water. Therefore, the best way to maintain the specific surface area of ZnO-M is to keep it in the dark under an inert atmosphere.
- The presence of oxygen in a dry atmosphere (either air or 21%O_2/He) causes similar losses of specific surface area, regardless of the lighting conditions or the type of atmosphere (average specific surface area loss: 21.4 ± 6.4%). Thus, CO_2 in air does not affect the loss of specific surface area under dry conditions.
- The presence of water in a CO_2-free atmosphere (either He or 21%O_2/He) causes similar losses of specific surface area, regardless of the lighting conditions or the type of atmosphere (average specific surface area loss: 31.5 ± 5.9%). Thus, O_2 does not produce an extra loss of specific surface area when water is present in the atmosphere. In other words, water is the prevailing agent that alters the surface area of polar ZnO. When CO_2 is present in the atmosphere (air), the loss of specific surface area increases up to 40.6 ± 4.9%. A more acidic environment, due to the presence of CO_2 and water, might even slightly accelerate the process.

The decrease in the I_{002}/I_{100} ratio during the unprotected storage of ZnO-P (inset in Figure 2B) suggests that crystal growth takes place more markedly at the expense of polar surfaces. It can be concluded that the nanosheets are formed by more or less rounded nanoparticles that are preferably oriented so that their polar (002) planes mostly show up on the main surfaces of the nanosheets, whereas the narrow edges are primarily formed by (100) planes. During storage the ZnO crystals grow mainly due to the partial merging of their polar surfaces at the expense of the narrow mesoporosity in a process triggered by the action of moisture, oxygen and, in their absence, light.

The crystallinity of the samples (DOC) increases slightly during unprotected storage (from 63% to 68% for ZnO-M and from 78% to 83% for ZnO-P, after 10 days' storage).

Conclusions

The room temperature sintering of polar ZnO nanosheets of high specific surface area (~120 m^2/g) has been analyzed under different atmospheres. During storage in lab conditions the nanosheets lost up to 75% of their specific surface area in about two months, with most of the reduction taking place during the first two weeks. Loss of surface area occurred parallel to the growth of nanocrystals, mainly due to the partial merging of their polar surfaces at the expense of the fraction of small mesopores (~5 nm pore size) initially present in the nanosheets. No decrease or increase in weight was detected during the process. Under the flow of different gases, the highest loss of specific surface area after 4 days occurred with moist air (with or without light), ~41%, followed by a moist CO_2-free atmosphere (with or without light and/or oxygen), ~32%; then a dry CO_2-free oxygen-containing atmosphere (with or without light), ~21%; then a dry inert atmosphere with light, ~15%; and finally a dry inert atmosphere in darkness, ~5%.

Acknowledgements

The financial support for this research work provided by the Spanish MINECO (CTM2014-56770-R project) and FEDER Funds (GRUPIN14-102, Principado de Asturias) is gratefully acknowledged. AFP is grateful to the Spanish MINECO for the award of a contract (BES-2015-072274).

Reference list

[1] S. Baruah, J. Dutta, Hydrothermal growth of ZnO nanostructures, Science and Technology of Advanced Materials, 10 (2009) 1-18.

[2] S. Maiti, S. Pal, K.K. Chattopadhyay, Recent advances in low temperature, solution processed morphology tailored ZnO nanoarchitectures for electron emission and photocatalysis applications, CrystEngComm, 17 (2015) 9264-9295.
[3] Y.-K. Peng, L. Ye, J. Qu, L. Zhang, Y. Fu, I.F. Teixeira, I.J. McPherson, H. He, S.C.E. Tsang, Trimethylphosphine-Assisted Surface Fingerprinting of Metal Oxide Nanoparticle by 31P Solid-State NMR: A Zinc Oxide Case Study, Journal of the American Chemical Society, 138 (2016) 2225-2234.
[4] H. Zhang, J. Sun, C. Liu, Y. Wang, Distinct water activation on polar/non-polar facets of ZnO nanoparticles, Journal of Catalysis, 331 (2015) 57-62.
[5] D.F. Wang, T.J. Zhang, Study on the defects of ZnO nanowire, Solid State Communications, 149 (2009) 1947-1949.
[6] H. Wilmer, M. Kurtz, K.V. Klementiev, O.P. Tkachenko, W. Grunert, O. Hinrichsen, A. Birkner, S. Rabe, K. Merz, M. Driess, C. Woll, M. Muhler, Methanol synthesis over ZnO: A structure-sensitive reaction?, Physical Chemistry Chemical Physics, 5 (2003) 4736-4742.
[7] T.T. Vu, L. del Río, T. Valdés-Solís, G. Marbán, Stainless steel wire mesh-supported ZnO for the catalytic photodegradation of methylene blue under ultraviolet irradiation, Journal of Hazardous Materials, 246-247 (2013) 126-134.
[8] T.T. Vu, L. del Río, T. Valdés-Solís, G. Marbán, Fabrication of wire mesh-supported ZnO photocatalysts protected against photocorrosion, Applied Catalysis B: Environmental, 140–141 (2013) 189-198.
[9] T.T. Vu, G. Marbán, Sacrificial template synthesis of high surface area metal oxides. Example: An excellent structured Fenton-like catalyst, Applied Catalysis B: Environmental, 152–153 (2014) 51-58.
[10] T.T. Vu, A.B. Rodil, G. Marbán, T. Valdés-Solís, Nanostructured stainless steel wire mesh-supported $Cd_xZn_{1-x}O$: A stable photocatalyst under visible and ultraviolet irradiation, Journal of Environmental Chemical Engineering, 2 (2014) 1612-1620.
[11] D. Wakuda, M. Hatamura, K. Suganuma, Novel method for room temperature sintering of Ag nanoparticle paste in air, Chemical Physics Letters, 441 (2007) 305-308.
[12] D. Wakuda, K.-S. Kim, K. Suganuma, Room temperature sintering of Ag nanoparticles by drying solvent, Scripta Materialia, 59 (2008) 649-652.
[13] K. Black, J. Singh, D. Mehta, S. Sung, C.J. Sutcliffe, P.R. Chalker, Silver Ink Formulations for Sinter-free Printing of Conductive Films, Scientific Reports, 6 (2016) 20814.
[14] M. Kruk, M. Jaroniec, A. Sayari, Application of large pore MCM-41 molecular sieves to improve pore size analysis using nitrogen adsorption measurements, Langmuir, 13 (1997) 6267-6273.
[15] X.-G. Han, H.-Z. He, Q. Kuang, X. Zhou, X.-H. Zhang, T. Xu, Z.-X. Xie, L.-S. Zheng, Controlling Morphologies and Tuning the Related Properties of Nano/Microstructured ZnO Crystallites, The Journal of Physical Chemistry C, 113 (2009) 584-589.
[16] A. McLaren, T. Valdés-Solís, G. Li, S.C. Tsang, Shape and Size Effects of ZnO Nanocrystals on Photocatalytic Activity, Journal of the American Chemical Society, 131 (2009) 12540-12541.
[17] G.R. Li, T. Hu, G.L. Pan, T.Y. Yan, X.P. Gao, H.Y. Zhu, Morphology−Function Relationship of ZnO: Polar Planes, Oxygen Vacancies, and Activity, The Journal of Physical Chemistry C, 112 (2008) 11859-11864.
[18] F. Ansari, M. Ghaedi, M. Taghdiri, A. Asfaram, Application of ZnO nanorods loaded on activated carbon for ultrasonic assisted dyes removal: Experimental design and derivative spectrophotometry method, Ultrasonics Sonochemistry, 33 (2016) 197-209.
[19] M. Yin, Y. Gu, I.L. Kuskovsky, T. Andelman, Y. Zhu, G.F. Neumark, S. O'Brien, Zinc Oxide Quantum Rods, Journal of the American Chemical Society, 126 (2004) 6206-6207.
[20] L. Vayssieres, Growth of Arrayed Nanorods and Nanowires of ZnO from Aqueous Solutions, Advanced Materials, 15 (2003) 464-466.

[21] Z.R. Tian, J.A. Voigt, J. Liu, B. McKenzie, M.J. McDermott, M.A. Rodriguez, H. Konishi, H. Xu, Complex and oriented ZnO nanostructures, Nat Mater, 2 (2003) 821-826.
[22] H. Han, E. Sheng, Y. Ni, Y. Ma, N. Xiang, X. Ma, Sheet-tube-rod transformation for ZnO nanorods prepared by a simple reflux route, Materials Research Bulletin, 74 (2016) 21-26.
[23] Z. Zhu, T. Andelman, M. Yin, T.L. Chen, S.N. Ehrlich, S.P. O'Brien, Osgood, Jr., Synchrotron x-ray scattering of ZnO nanorods: Periodic ordering and lattice size, Journal of Materials Research, 20 (2005) 1033-1041.
[24] N. Kıcır, T. Tüken, O. Erken, C. Gumus, Y. Ufuktepe, Nanostructured ZnO films in forms of rod, plate and flower: Electrodeposition mechanisms and characterization, Applied Surface Science, 377 (2016) 191-199.
[25] D. Pradhan, K.T. Leung, Controlled Growth of Two-Dimensional and One-Dimensional ZnO Nanostructures on Indium Tin Oxide Coated Glass by Direct Electrodeposition, Langmuir, 24 (2008) 9707-9716.
[26] B. Santoshkumar, S. Kalyanaraman, R. Vettumperumal, R. Thangavel, I.V. Kityk, S. Velumani, Structure-dependent anisotropy of the photoinduced optical nonlinearity in calcium doped ZnO nanorods grown by low cost hydrothermal method for photonic device applications, Journal of Alloys and Compounds, 658 (2016) 435-439.
[27] T.T. Vu, L. del Río, T. Valdés-Solís, G. Marbán, Tailoring the synthesis of stainless steel wire mesh-supported ZnO, Materials Research Bulletin, 47 (2012) 1577-1586.
[28] C. Xiao, T. Yang, M. Chuai, B. Xiao, M. Zhang, Synthesis of ZnO nanosheet arrays with exposed (100) facets for gas sensing applications, Physical Chemistry Chemical Physics, 18 (2016) 325-330.
[29] D.B. Black, E.G. Lovering, Estimation of the degree of crystallinity in digoxin by X-ray and infrared methods, Journal of Pharmacy and Pharmacology, 29 (1977) 684-687.

Captions to figures

Figure 1. A) SEM image of ZnO-M; B) SEM image of ZnO-P.

Figure 2. A) XRD spectra at different storage times (unprotected storage) for ZnO-M; B) XRD spectra at different storage times (unprotected storage) for ZnO-P. Insets in Figs. 2A and 2B: variation of d_{XRD} and I_{002}/I_{100} with storage time for ZnO-M and ZnO-P, respectively.

Figure 3, Effect of polarity (anisotropy) and orientation on the intensity of the XRD peaks for single crystalline wurtzite-type ZnO nanostructures.

Figure 4. A) TEM image of the main surface of a freshly calcined ZnO nanosheet; B) SAED analysis of this surface; C) TEM image showing the narrow mesopores of the nanosheet.

Figure 5. N_2 physisorption isotherms for the freshly calcined ZnO-M and for the same sample after it has been stored for 40 days in lab conditions. Inset: Pore size distributions of the samples.

Figure 6. Variation of the specific surface area loss for ZnO-M stored under lab conditions.

Figure 7. Values of specific surface area loss for ZnO-M after 4 days of storage under a flow (100 mL/min) of different gases and under different lighting conditions.

Figures

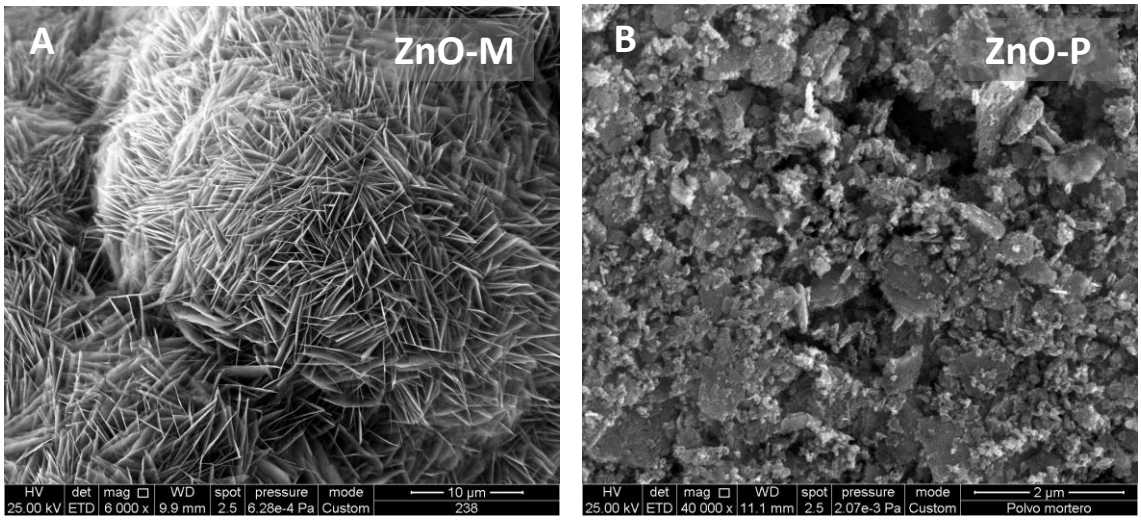

Figure 1

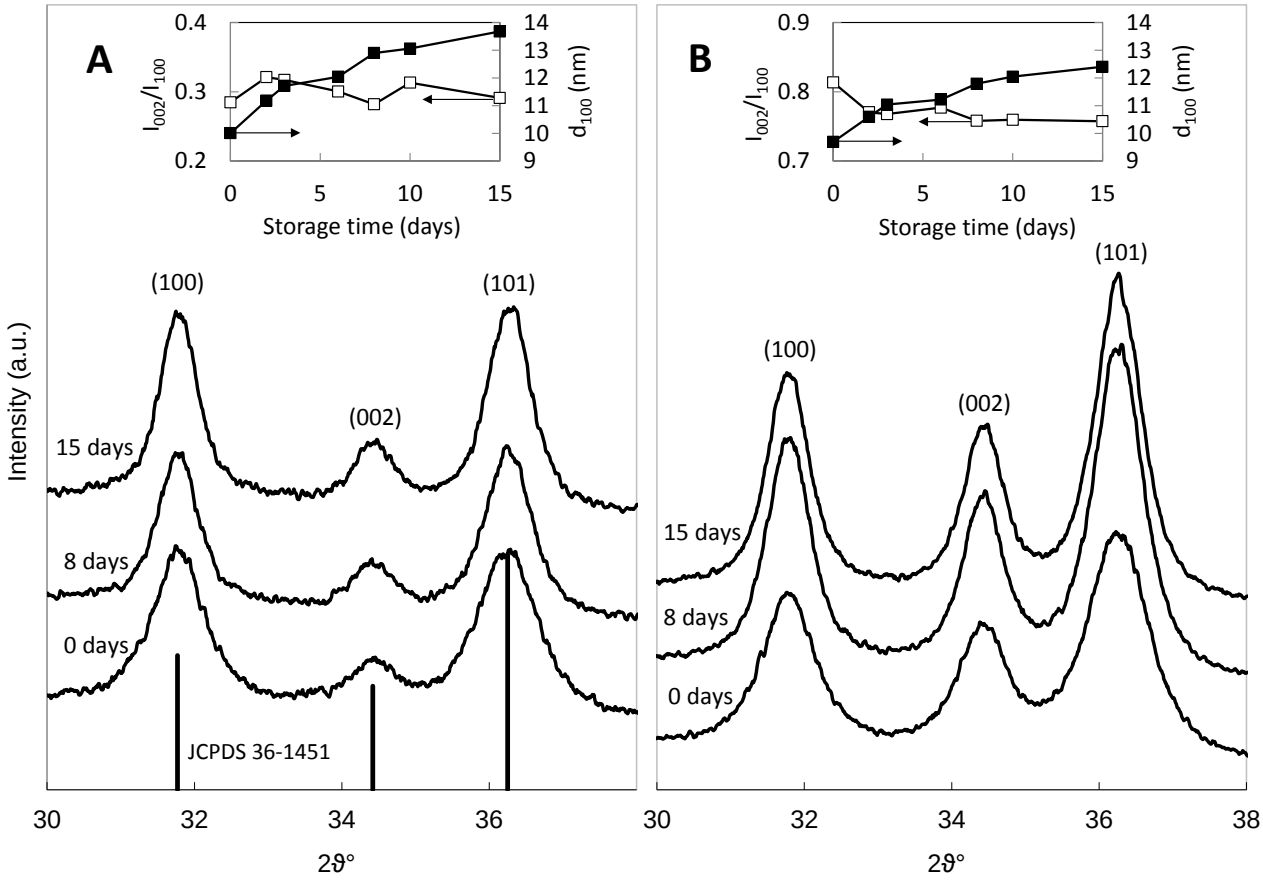
A
B
I_{002}/I_{100}
d_{100} (nm)
Storage time (days)
(100)
(002)
(101)
15 days
8 days
0 days
JCPDS 36-1451
Intensity (a.u.)
2ϑ°

Figure 2

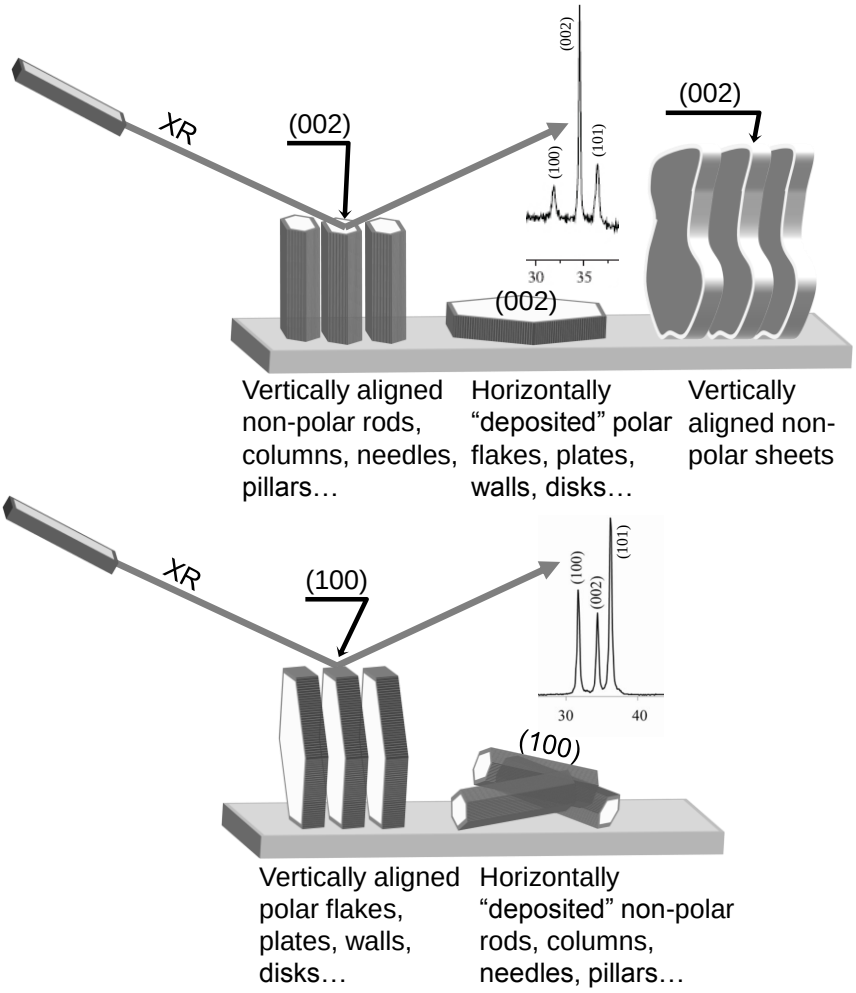
XR
(002)
(002)
(100)
(101)
30
35
(002)
Vertically aligned non-polar rods, columns, needles, pillars…
Horizontally “deposited” polar flakes, plates, walls, disks…
Vertically aligned non-polar sheets
XR
(100)
(100)
(002)
(101)
30
40
(100)
Vertically aligned polar flakes, plates, walls, disks…
Horizontally “deposited” non-polar rods, columns, needles, pillars…

Figure 3

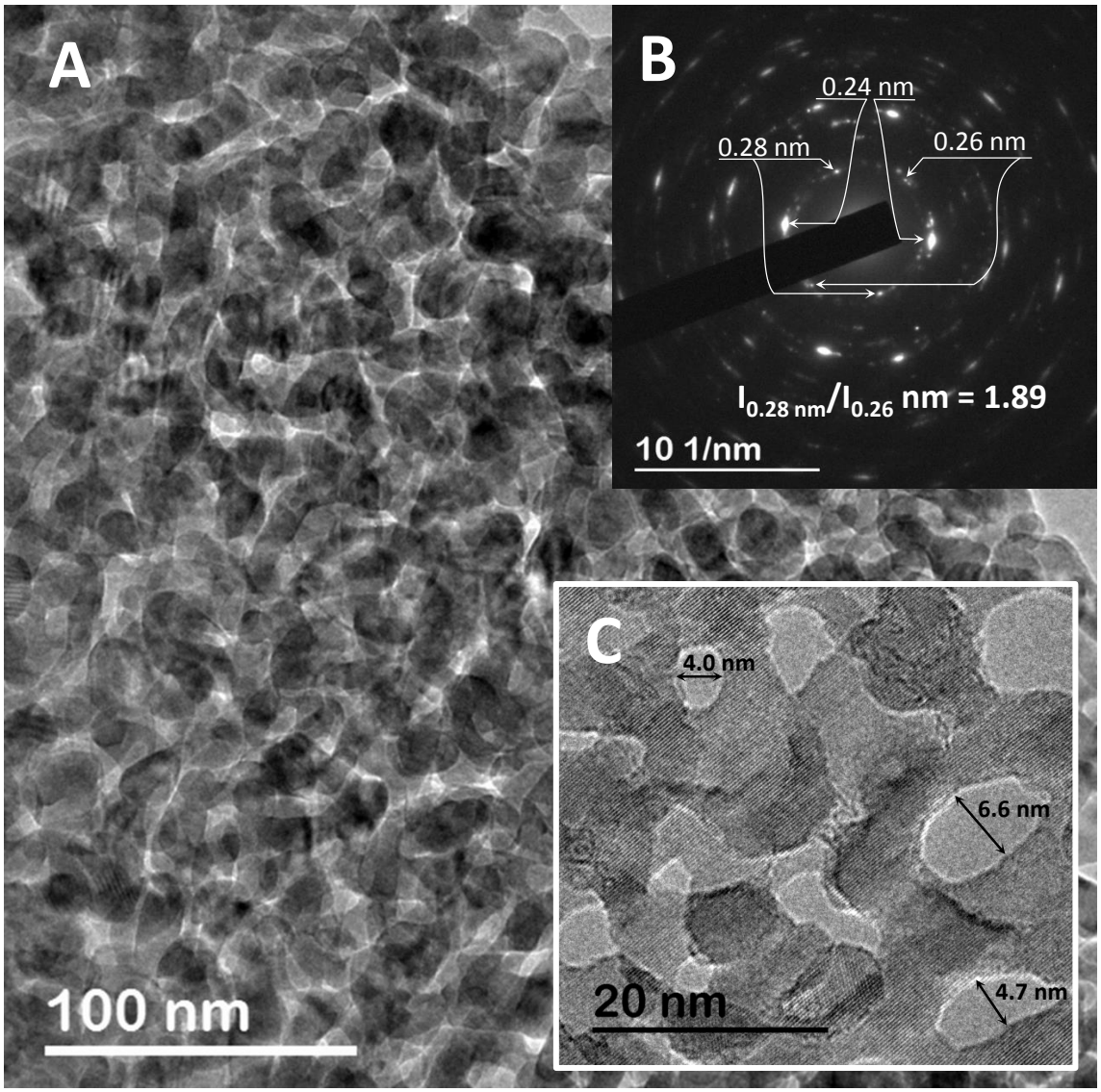
A
100 nm
B
0.24 nm
0.28 nm
0.26 nm
$I_{0.28\ nm}/I_{0.26}$ nm = 1.89
10 1/nm
C
4.0 nm
6.6 nm
4.7 nm
20 nm

Figure 4

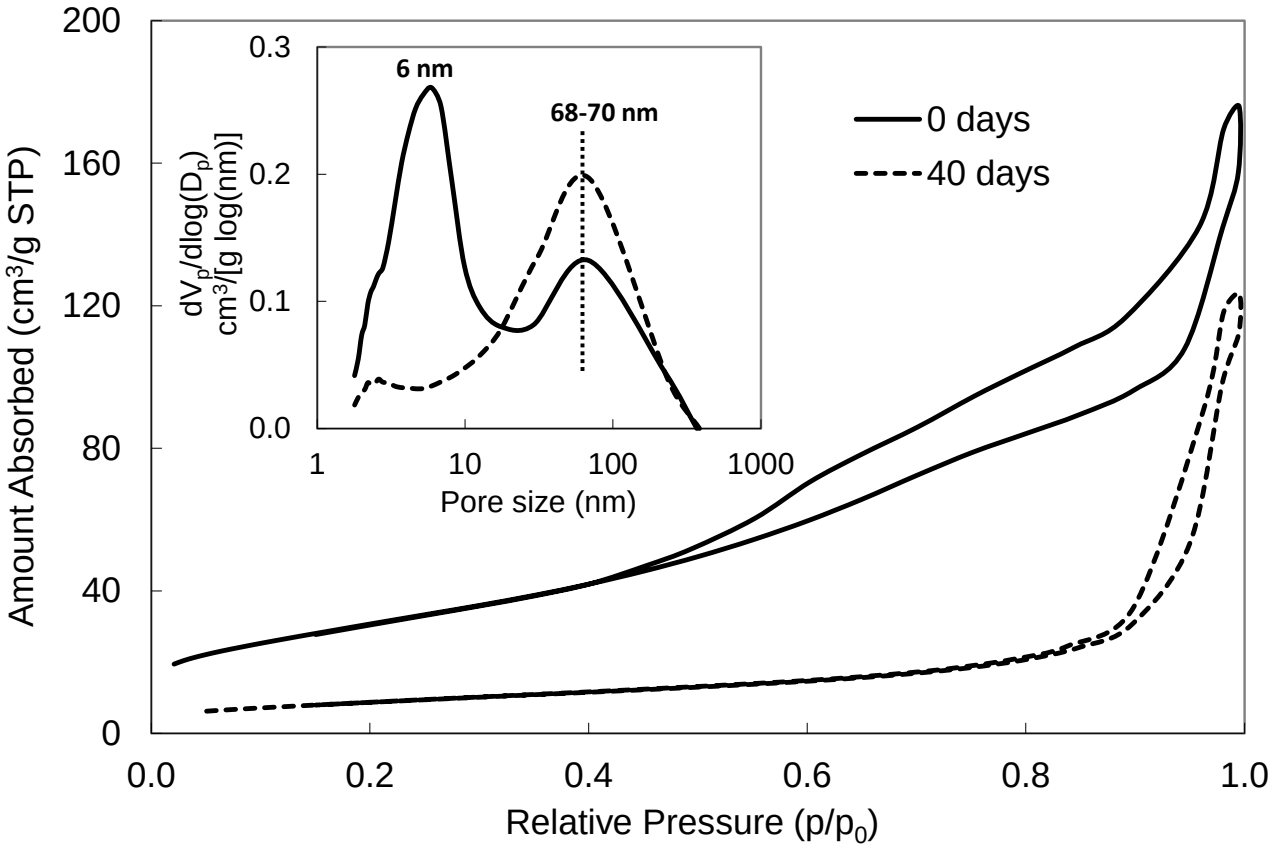
Amount Absorbed (cm3/g STP)
Relative Pressure (p/p0)
0 days
40 days
6 nm
68-70 nm
dVp/dlog(Dp) cm3/[g log(nm)]
Pore size (nm)

Figure 5

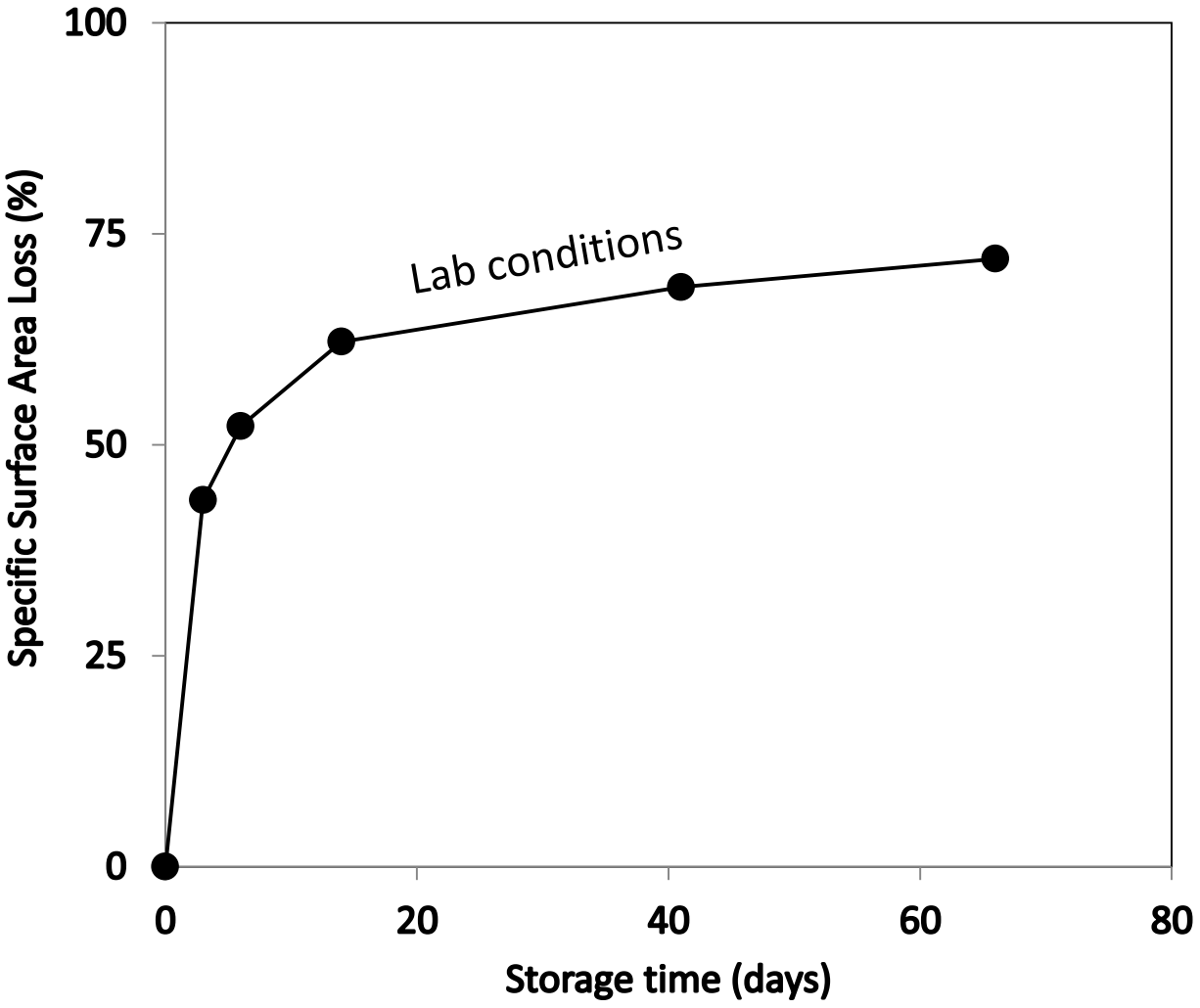
100
75
50
25
0
Specific Surface Area Loss (%)
Lab conditions
0
20
40
60
80
Storage time (days)

Figure 6

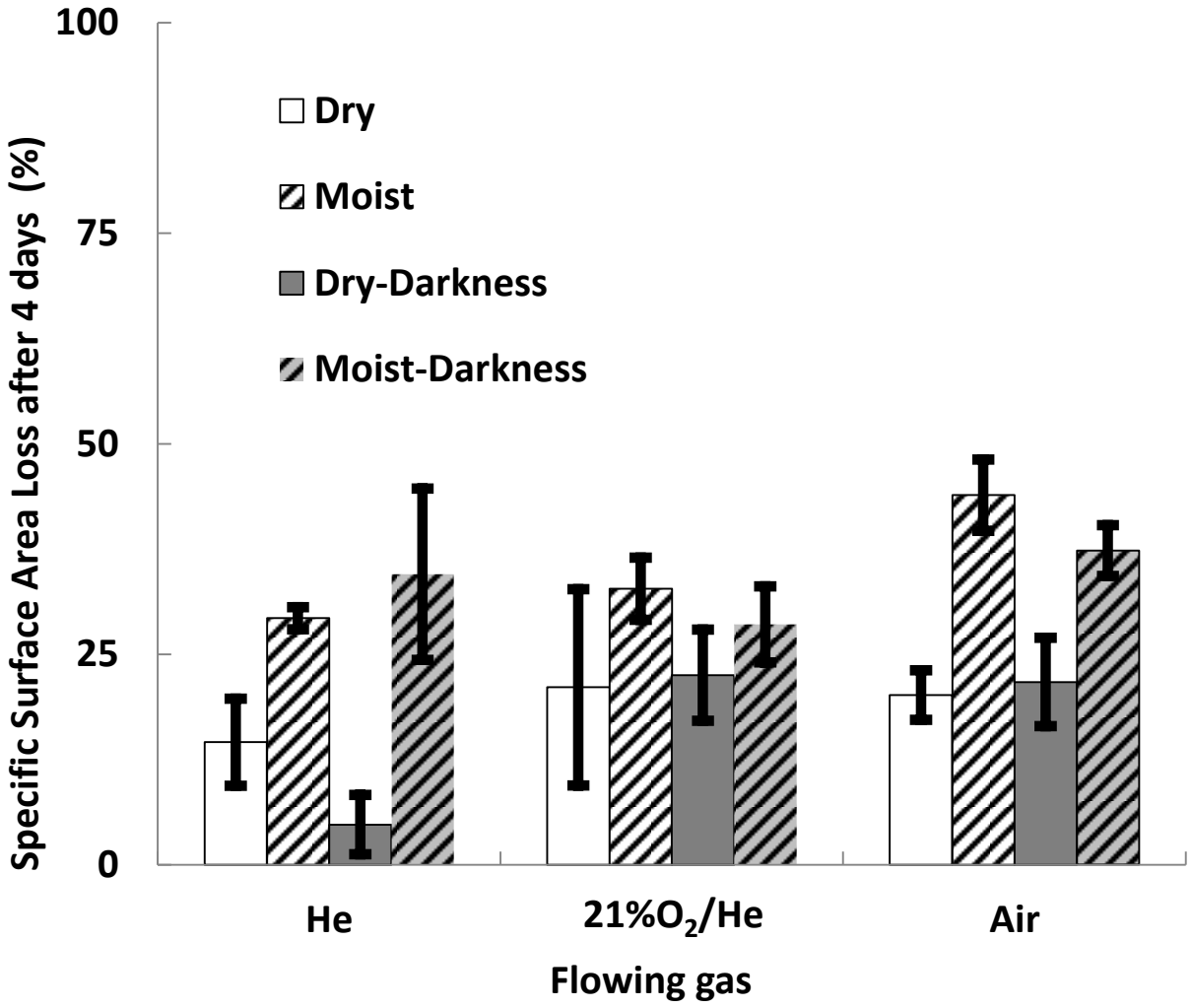
100
75
50
25
0
Specific Surface Area Loss after 4 days (%)
Dry
Moist
Dry-Darkness
Moist-Darkness
He
21%O2/He
Air
Flowing gas

Figure 7